

MODELING AND MECHATRONIC DESIGN OF MECHANISMS WITH FLEXIBLE JOINTS, design of an active encoderhead

J.van Dijk, R.G.K.M. Aarts, J.B.Jonker

October 16, 2009

Abstract: The relationship between the required frequency of higher order dynamics and the required control bandwidth based on the small-gain theorem will be presented. The relationship is important in mechatronic system design. It will be shown that the relationship needs adequate 3D dynamic system modeling. The models used in an early conceptual phase of the mechatronic design should not be un-necessary complex or time-consuming. One or two dimensional lumped parameter models can be used for their simplicity. However, even for rather simple mechanical systems such models may ignore relevant three-dimensional or non-linear effects. Models obtained with a standard linear finite element method often need many elements to achieve sufficient accuracy.

In this paper analyses with a multibody approach based on non-linear finite elements is discussed. Due to the sound inclusion of the non-linear effects at the element level only a rather small number of elastic beam elements are needed to model typical components accurately. Configuration dependent linearized models can be generated for control system design. This approach is offered by the SPACAR software package and its applicability is demonstrated for the design of an active encoderhead. The effects of e.g. non-linearities, manufacturing imperfections and violation of exact constraint design on relevant natural frequencies are analyzed easily and quickly with the low-order and accurate models offered by the modeling approach.

1 Introduction

The paper deals with the mechatronic design of mechanisms with flexible joints applied in the field of precision equipment. The contribution of the paper is on conceptual design using adequate state space models describing the spatial system dynamics. The necessary theoretical considerations of mechatronic design are described. It will be shown that exact constraint design [2] is important for reliable dynamic behavior. Another important dynamics related issue of mechatronic design is the influence of higher order dynamics. This influence can be easily judged without the need of complicated models. The small-gain theorem [7] is used to derive a clear relationship between requirement for system's higher order dynamics and the required control bandwidth. For this reason a convenient controller parametrization will also be presented. The relationship needs

adequate 3D dynamic system modeling.

The modeling of the systems under consideration becomes more complicated as the dynamic properties like natural frequencies and buckling performance may vary considerably in between the extreme positions. This is especially the case when flexible joints are used. They offer the advantages of low friction and no backlash. However, in cases where these mechanisms have to realize relatively large motions, the joints are designed to undergo relatively large elastic deformations and non-linear effects strongly affect the system's performance.

In an early conceptual phase of the mechatronic design process the designer would like to use models that on the one hand capture the dominant, possibly varying system behavior while on the other hand complicated models should be avoided as these are too time-consuming. Lumped parameter models are relatively simple and can capture some of the dominant one or two dimensional behavior, but three dimensional effects, such as the influence of mode-shapes on the sensor-output, are usually not fully taken into account. Linear finite element analyses are better suited to reveal this more complicated behavior, yet at the expense of a rather large number of degrees of freedom. Furthermore, the analysis near the unloaded equilibrium position may be straightforward, non-linear effects, such as geometrical stiffening, have to be accounted for to analyze the systems behavior accurately in the full operating range. Common linear finite element analyses often do not account correctly for the complete non-linear behavior and/or are very time consuming. In this paper we discuss the use of the SPACAR software, in particular applied for mechatronic design. It offers a multi-body approach based on non-linear finite elements of which details have been published [6]. The sound inclusion of the non-linear effects, such as geometrical stiffening, at the element level appears to be very advantageous. Only a rather small number of elastic beam elements is needed to model e.g. a leaf spring accurately. The non-linear model can be linearized in a number of configurations throughout the complete operational range of the mechanism to obtain a series of locally linearized models, e.g. state space models for control system design of the linear time-varying system [6]. Numerically efficient models are obtained as the number of degrees of freedom is rather small. Consequently, the approach is particularly well suited during the early (mechatronic) design phase, where time consuming computations would severely hamper the design progress. The software has a user-friendly graphical user interface with which the models can be created easily [1]. For further processing and e.g. control system design the modelling results can be easily imported in MATLAB/SIMULINK.

In this paper the applicability will be illustrated considering a simple example with design goals as are outlined next. The effects of e.g. non-linearities, manufacturing imperfections and violation of exact constraint design on relevant natural frequencies are shown and analyzed easily and quickly with the low-order and accurate models.

Example System

A mobile radar system is capable of searching and pointing. In both operating modes the angular position of the radar is determined by reading out an optical encoder system which is mounted inside the cylindrical base of the radar. The diameter d of the ring is about 1 m. A high resolution grating tape is mounted in the ring (figure 1). The encoder head detects relative movements of the grating tape and ring ([5]). For a high accuracy and reliability the distance

between head and ring needs to remain within strict tolerances. However, the geometrical imperfections of the ring of the base and the deformations due to vibrations are such that the tolerance on the distance between encoder head and encoder grating-tape are not achieved. A previous solution is to mount the head on guiding wheels which are in contact with the ring in which the tape is mounted. In this way the distance is kept constant. But due to the direct contact the solution suffers from wear. Therefore, a solution is investigated and realized which keeps the head on a constant distance from the tape without contact by making the head active and using an inductive sensor to measure the gap distance. We describe the design procedure and report the influences of violation of exact constrained design, limited manufacturing tolerances and parasitic modes on the robust stability of the closed loop.

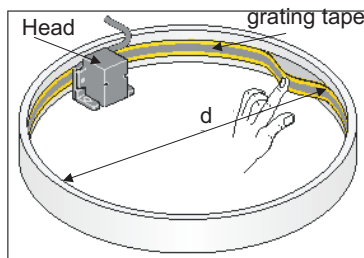


Figure 1: Encoder system

First we describe some theoretical aspects of the mechatronic design procedure in section 2. In section 3 the conceptual design of the active encoder head system, controller design and determination of necessary cross-over frequency is outlined. In section 4 the mechanical design of the straight guidance is described. Section 5 is dedicated to the modeling of the example using SPACAR. Section 6 contains the description of the robust stability check using these models and the theorem of section 2. Section 7 contains some concluding remarks. The most important conclusion is that a combination of manufacturing tolerances and violation of exact constraint design are of great influence on the behavior and therefore performance of the example system.

2 Theoretical background on mechatronic design

In the following subsections controller parametrization and robust stability will be addressed.

2.1 Control parametrization

In this section we will show that P(I)D controllers for electro-mechanical systems can be parameterized in such way that all parameters are dependent on one variable only, namely the cross-over frequency. The cross-over frequency is

determined by the required performance of the controlled system. This performance is either a required disturbance rejection, or a demand on the error in case of a set-point change in point to point motion systems, or a demand on reference tracking in servo-systems.

2.1.1 The plant to control

Controlled electro-mechanical systems can be seen as a mechanical subsystem that is driven by an actuator delivering force in order to move the subsystem to a desired position. Most of the time the actuator is an inductive actuator applied with either voltage- or current-mode power amplification. For control synthesis the mass of the subsystem to move is considered rigid. A one dimensional model will be adequate for performance analyses. As a consequence we end up with the simple model shown in figure 2.

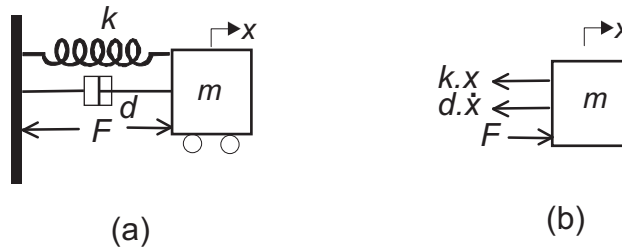


Figure 2: Nominal Model, a) Ideal Physical Model, b) Free body diagram

In figure 2 k is the stiffness in actuated direction, m is the mass to move, F is the force supplied by the actuator and d is the damping constant. From figure 2b the equation of motion can be obtained:

$$m \cdot \ddot{x} = -k \cdot x - d \cdot \dot{x} + F \quad (1)$$

The basic transfer function between position of the mass x and actuator-force F is then described by

$$\frac{x(s)}{F(s)} = P(s) = \frac{1}{ms^2 + ds + k} \quad (2)$$

where s is the Laplace-operator. In case of voltage control the force

$$F = \frac{U \cdot k_m}{R} \quad (3)$$

where U is the applied voltage by the power amplifier, k_m the motor constant, and R the resistance of the coil. In that case:

$$d = \frac{k_m^2}{R} \quad (4)$$

is the damping due to back-emf. In current mode control, $F = k_m \cdot i$ and the assumption $d = 0$ is made. The current applied by the power amplifier is denoted by i .

In case the mechanical subsystem does not have stiffness in the actuated direction $k = 0$. Usually the stiffness k is desired to be low. Therefore, the first resonance frequency in (2) $\omega_1 = \sqrt{\frac{k}{m}}$ is low or zero. Consequently, at higher frequencies ($\omega > \omega_1$) (2) can be approximated by:

$$\frac{x(s)}{F(s)} = P(s) = \frac{1}{ms^2} \quad \forall \quad \omega > \omega_1 \quad (5)$$

In case of voltage control (5) becomes:

$$\frac{x(s)}{U(s)} = P(s) = \frac{c_u}{ms^2} \quad \forall \quad \omega > \omega_1 \quad (6)$$

and in case of current control (5) becomes:

$$\frac{x(s)}{i(s)} = P(s) = \frac{c_i}{ms^2} \quad \forall \quad \omega > \omega_1 \quad (7)$$

with $c_u = k_m/R$ and $c_i = k_m$.

2.1.2 P(I)D controllers

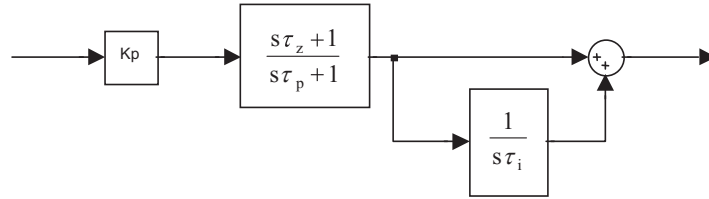


Figure 3: Block-diagram of PID-controller

A simple PID-controller is a parallel connection of a PD-controller and a separate I-action, as shown in figure 3. The transfer-function of this P(I)D-controller is:

$$K(s) = k_p \cdot \left(\frac{s\tau_z + 1}{s\tau_p + 1} \right) \cdot \left(1 + \frac{1}{\tau_i s} \right) \quad (8)$$

We can rewrite the expression (8) to:

$$K(s) = k_p \cdot \frac{(s\tau_z + 1)(s\tau_i + 1)}{s\tau_i(s\tau_p + 1)} \quad (9)$$

Figure 4 shows the bode-diagram of this P(I)D-controller.

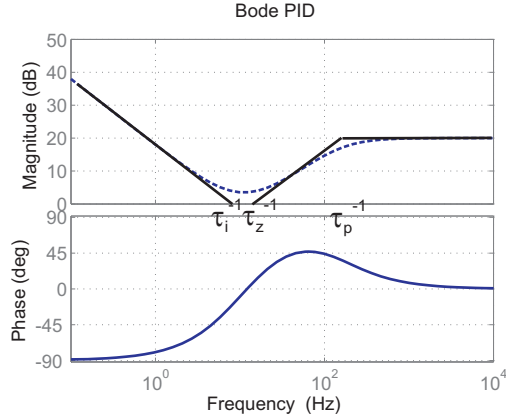


Figure 4: Bode diagram of PID-controller

Characteristic for the PID-controller is its high gain at low-frequencies. The first corner-point¹⁾ is determined by the transfer-zero in $\frac{1}{\tau_i}$ the second corner-point is determined by the transfer-zero in $\frac{1}{\tau_z}$. Finally, the gain at high frequency is limited by the de corner-point due to the pole in $\frac{1}{\tau_p}$. The corner-point $\frac{1}{\tau_z}$ in the frequency domain bode magnitude plot (see figure 4) indicates where the derivative action is started and $\frac{1}{\tau_p}$ indicates the corner-point where the derivative action stops. Since the I-action should be stopped before the derivative action starts, the corner-point $\frac{1}{\tau_i}$, indicating the stop of the integral-action, should be lower in frequency then the start of the derivative action. Therefore, usually $\tau_i = 2 \cdot \tau_z$.

Due the zero of the transfer in $\frac{1}{\tau_z}$, the PD-controller part provides phase-lead in a certain frequency range, as shown in figure 4. The amount of phase-lead at the cross-over frequency of the open-loop transfer is a measure for the amount of damping obtained by the dominant closed loop poles (see [4]). Next to that the P(I)D-controller is used to increase the initial cross-over frequency, and as a consequence, makes system respond faster.

In case the process transfer $P(s)$ yields equation (5) simple adjustment rules depending on the cross-over frequency ω_c can be derived. We replace τ_p in (9) by $\alpha \cdot \tau_z$ [4].

Referring to figure 4 the following can be concluded. The position of the second corner-point of the asymptote is determined by the location of the zero ($=\frac{1}{\tau_z}$). De position of the high frequent corner-point is determined by the location of the pole ($=\frac{1}{\tau_p}$).

The maximum gain of the P(I)D-controller at high frequencies is determined by $(\lim_{s \rightarrow \infty} K(s))$

$$|K|_{hf} = k_p \left(\frac{\tau_z}{\tau_p} \right) \quad (10)$$

¹⁾The point where the asymptote is turning into a line with different angle. Also sometimes called turning-point for that reason

The maximum phase-lead is obtained at a frequency of

$$\omega_{ph_{max}} = \log^{-1} \frac{\log \frac{1}{\tau_z} + \log \frac{1}{\tau_p}}{2} = \sqrt{\frac{1}{\tau_z \cdot \tau_p}} \quad (11)$$

The amount of phase-lead is determined by the ratio $\frac{\tau_z}{\tau_p} = \frac{1}{\alpha}$.

The gain of the P(I)D-controller at the frequency where the maximum phase-lead is obtained is:

$$|K|_{ph_{max}} = k_p \left(\sqrt{\frac{1}{\alpha}} \right) \quad (12)$$

The maximum phase-lead is at $\omega = \omega_{ph_{max}}$ (11). As a consequence, we need to design the P(I)D-controller in such a way that this frequency, where maximum phase-lead is obtained, is located at the desired cross-over frequency (ω_c) of the open-loop system. Using (11) the following relation between τ_z and ω_c can then be obtained:

$$\begin{aligned} \omega_c &= \sqrt{\frac{1}{\tau_z \cdot \tau_p}}, \\ &= \frac{1}{\tau_z} \cdot \sqrt{\frac{1}{\alpha}}, \\ \tau_z &= \frac{1}{\omega_c} \cdot \sqrt{\frac{1}{\alpha}} \end{aligned} \quad (13)$$

Furthermore, $\tau_p = \alpha \cdot \tau_z$. Using this expression we can easily write τ_p as:

$$\tau_p = \alpha \cdot \tau_z \rightarrow \tau_p = \frac{1}{\sqrt{\frac{1}{\alpha}} \cdot \omega_c} \quad (14)$$

The cross-over frequency is the point in the bode-diagram where by definition the open-loop gain is 1. $\|KG\| = 1$. Consequently:

$$\begin{aligned} \|K \cdot G\|_{\omega_c} &= \left\| \frac{K(j\omega_c) \cdot c}{m \cdot (j\omega_c)^2} \right\| = \frac{k_p \sqrt{\frac{1}{\alpha}}}{m_{eq} \omega_c^2} = 1 \rightarrow \\ k_p &= \frac{m_{eq} \omega_c^2}{\sqrt{\frac{1}{\alpha}}} \end{aligned} \quad (15)$$

where we have used (5) and c is either c_u or c_i , for simplicity we have defined $m_{eq} = \frac{m}{c}$. By these argumentations we have shown the adjustment-rules:

$$\begin{aligned} \tau_z &= \frac{\sqrt{\frac{1}{\alpha}}}{\omega_c} \\ \tau_i &= 2 \cdot \tau_z \\ \tau_p &= \frac{1}{\sqrt{\frac{1}{\alpha}} \cdot \omega_c} \\ k_p &= \frac{m_{eq} \cdot \omega_c^2}{\sqrt{\frac{1}{\alpha}}} \end{aligned} \quad (16)$$

A slight modification to the P(I)D-controller of (9) is the so called P(I)D⁺-controller. The P(I)D⁺-controller has one degree of roll-off at higher frequencies

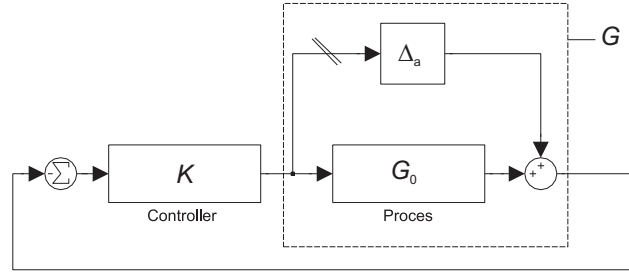


Figure 5: Additive uncertainty model

and is described by:

$$\frac{u(s)}{e(s)} = K(s) = k_p \frac{(s\tau_z + 1)(s\tau_i + 1)}{s\tau_i(s^2\tau_p^2 + 2\zeta\tau_p s + 1)} \quad (17)$$

Usually $\zeta = 0.7 - 0.9$ in (17). This type of controller gives more safety against instability due to higher order dynamics.

2.2 Robust stability

Because, we wish to not to bother too much about higher order dynamics of the plant to control, the controller is usually designed on a low order nominal model. More complex models will show vibration modes due to the elasticity but it is assumed that these modes do not influence the performance but they have only influence on the robust stability. Remark, that performance is usually a low frequent phenomena and stability is usually a high frequency issue. Low order models have at low frequency a good fit with the real system.

Question is, whether are not in the feedback loop, based on the real problem with the controller designed on the nominal model, still a stable loop? In other words provides the designed controller robust stability? More insight is necessary and this is provided by the application of the small gain theorem.

In figure 5 the actual plant (dashed box) is modeled using a nominal model and an additive uncertainty model. The relations for this additive model of unstructured uncertainty can be written as:

$$\begin{aligned} G(s) &= G_0(s) + \Delta_a(s), \\ \Delta_a &= W_a \tilde{\Delta}_a, \\ \|\tilde{\Delta}_a\|_\infty &\leq 1, \end{aligned} \quad (18)$$

where $G(s)$ is the actual plant and $G_0(s)$ is the nominal model of the plant. $W_a(s)$ is a stable filter modeling the additive uncertainty $G(s) - G_0(s)$, $\tilde{\Delta}_a$ is a perturbation of unity magnitude.

Breaking the loop just before the additive uncertainty model at the indicated position results in the loop gain:

$$Q = -W_a(I + G_0K)^{-1}K \quad (19)$$

To check whether the feedback system will remain stable under the perturbations, we need to check whether the feedback combination of Q (19) and $\tilde{\Delta}_a$ will remain stable for all allowable $\tilde{\Delta}_a$. We know that Q is stable (since K stabilizes G_0) and we assume $\tilde{\Delta}_a$ is stable. Then the feedback system can become unstable only if one or more of the characteristic loci of $-Q\tilde{\Delta}_a$ encircles the point -1. In [7] it is shown that:

$$\rho(Q\tilde{\Delta}_a) \leq \bar{\sigma}(Q\tilde{\Delta}_a) \quad (20)$$

In (20) $\rho(\cdot)$ denotes the spectral radius, and so no encirclement of -1 can occur if, at each frequency:

$$\bar{\sigma}(Q\tilde{\Delta}_a) < 1 \quad (21)$$

In (21) $\bar{\sigma}$ denotes the largest singular value. If we model $W_a(s)$ in such a way that $\|\tilde{\Delta}_a\|_\infty \leq 1$ then (21) is equivalent with:

$$\bar{\sigma}(Q) < 1 \quad (22)$$

This is a sufficient condition to guarantee that instability can not occur for any of the possible perturbations. Remark, that (22) is obtained for unstructured uncertainty. However, if the structure of the uncertainty is known and for example has a block structure, then the condition (22) is too stringent. Because a lot of the perturbations satisfying $\|\tilde{\Delta}_a\|_\infty \leq 1$ are no longer permissible. Then condition (22) changes to:

$$\mu(Q) < 1 \quad (23)$$

where $\mu(\cdot)$ is the structured singular value of the interconnection-matrix Q given a particular structure of $\tilde{\Delta}_a$.

For analyzing instability of small input output systems due to neglected higher order dynamics, we rely on (22). Which can be rewritten into the following form:

$$\begin{aligned} \bar{\sigma}(W_a(I + G_0K)^{-1}K) < 1 \rightarrow \\ \bar{\sigma}(W_a) < \bar{\sigma}(K^{-1}) \quad \forall \quad \omega > \omega_c \end{aligned} \quad (24)$$

where we have made the following simplifications. Considered is that beyond the cross-over frequencies $|G_0K|$ is small compared to the unity matrix I. We used $\bar{\sigma}(W_aK) < \bar{\sigma}(W_a) \cdot \bar{\sigma}(K)$. Moreover, beyond the cross-over frequency at the resonance frequencies $\bar{\sigma}(W_a) \approx \bar{\sigma}(G)$. This leads to the quick robustness check:

$$\bar{\sigma}(G) < \bar{\sigma}(K^{-1}) \quad \forall \quad \omega > \omega_c \quad (25)$$

From this MiMo quick robustness check (25) we can derive for the SiSo case the following.

$$G(j\omega) < K(j\omega)^{-1} \quad \forall \quad \omega > \omega_c \quad (26)$$

The resonances in the bodeplot of $G(s)$ should stay at frequencies $\omega > \omega_c$ below the bodeplot of the inverse of the controller $K(s)$. For $\omega > \omega_c$ the P(I)D-controller (9) is approximated by:

$$K_{HF} = \frac{k_p \cdot \tau_z}{\tau_p} = \frac{k_p}{\alpha} = \frac{m_{eq}\omega_c^2}{\sqrt{\alpha}} \quad (27)$$

where we have used the controller parametrization (16). The transfer function of a plant with at least one resonance mode with frequency ω_r is described by:

$$G(s) = \frac{1}{m_{eq} \cdot s^2} \cdot \frac{\omega_r^2}{s^2 + 2\zeta\omega_r s + \omega_r^2} \quad (28)$$

Since the resonance in the bodeplot of $G(s)$ should stay at frequencies $\omega > \omega_c$ below the bodeplot of the inverse of the controller $K(s)$, we analyze at $s = j\omega_r$ the magnitude of the transfer (28):

$$G(j\omega_r) = \left| \frac{1}{m_{eq} 2\zeta\omega_r^2} \right| \quad (29)$$

From (26) we can derive the rule of thumb:

$$\left| \frac{1}{m_{eq} 2\zeta\omega_r^2} \right| < \frac{\sqrt{\alpha}}{m_{eq}\omega_c^2}, \quad \omega_r > \omega_c \sqrt{\frac{1}{2\zeta\sqrt{\alpha}}} \quad (30)$$

Note, that in the case of the application of a P(I)D⁺-controller this rule becomes:

$$\omega_r > \omega_c \sqrt[3]{\frac{1}{2\zeta\alpha}} \quad (31)$$

3 Specifications and conceptual design of the example system

In here the specifications of the example systems are rewritten to a cross-over requirement for the open-loop transfer $G(s) \cdot K(s)$. Next, the conceptual design of the active encoder head system and the controller design are outlined.

3.1 Specifications

Due to the high angular resolution demands (< 0.03 mrad) the gap between head and tape has a tolerance of 0.2 mm. The geometrical imperfections can be expressed in worst case as an eccentricity with 0.3 mm amplitude. The searching angular speed of the radar is 2π rad/sec. The worst case amplitude of the gap-width due to vibrations is 0.4 mm. The corresponding vibration mode has a frequency of 10 Hz. As a consequence we have to reduce a disturbance with a frequency of 10 Hz. and an amplitude of 0.7 mm in closed loop to result an error with a maximum amplitude of 0.1 mm.

Figure 6 shows a block-diagram of the closed loop system with disturbance d . In here K is the transfer-function of the controller and P the transfer-function of the proces. The error in the gap-width is denoted by e , the disturbance by d and the reference for the gap width by r . The closed loop transfer between d and e is the Sensitivity function S , for which we have implicitly specified:

$$\begin{aligned} \frac{e(s)}{d(s)} &= S(s) = \frac{-1}{1 + K(s)P(s)} \\ |S(j \cdot 2\pi \cdot 10)| &= \frac{1}{7} \end{aligned} \quad (32)$$

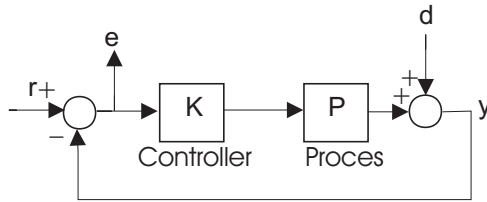


Figure 6: Closed loop blockdiagram

In the sequel the minus sign in (32) is left out, since only the magnitude of $S(s)$ is of concern.

The available volume for the mechanism of the active head is: $l \times w \times h = 100 \times 60 \times 60$ mm

3.2 Conceptual Design

A number of concepts for the mechanical part of the system are possible. However, in here we will restrict ourselves, due to there simple construction, to concepts with flexure guidance driven by a voice coil motor (VCM). Due to wear and maintenance of bearings, concepts with roller bearing guidance, spindle drives and rotary motors are not considered as options. Figure 7 shows three possible concepts with flexure guidance. In concepts (a) and (b) the flexures are wire springs and in concept (c) the flexures are leaf-springs. In order to guarantee straight guidance in the intended direction of motion (for short actuated direction) the stiffness of the flexures in all other direction except the actuated direction must be relatively high.

The drawback of these high stiffness demands is that it is not trivial to obtain both high compliance in actuated direction and high stiffness in other directions. Therefore, the stiffness properties should be optimized for low stiffness in actuated direction and robust stability for parasitic directions. As a consequence we need a low frequent mode in the actuated direction and high frequent modes in non actuated directions. Due to the fact that it's fabrication process is the simplest one, the leaf-spring concept is preferred.

However, it has an additional drawback. This concept suffers from a parasitic movement in the direction perpendicular to the actuated direction due to the leaf-springs. It is expected that this parasitic movement will not endanger the design.

3.3 Controller Design

3.3.1 Nominal Model

The nominal model to be used for controller design can now be established. In the nominal model the encoder-head will be considered as a simple rigid mass. Because the internal dynamics in the encoder-head will be high frequent compared to the frequencies of the support modes, due to the flexures, and the required bandwidth of the controller.

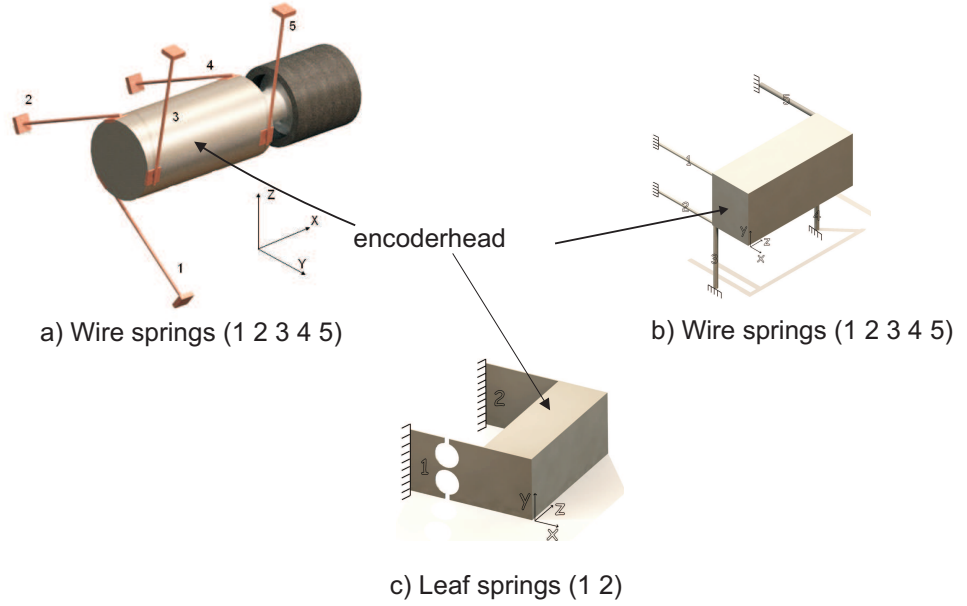


Figure 7: Concepts a) b) with wire springs, c) with leaf springs

A one dimensional model will be adequate for performance analyses. Because more complex 3D models will show modes due to the elasticity of the flexures but it is assumed that these modes do not have influence on the performance only on the robust stability. So these models will be investigated later. As a consequence we end up with the simple model as introduced in figure 2.

In here k is the stiffness in actuated direction due to the leaf springs, m is the mass of the encoder-head and sensor, F is the force supplied by the actuator and d is the damping which is due to the back-emf in the actuator. Because, the actuator will be fed by a voltage amplifier the actuator force is:

$$F = \frac{U \cdot k_m}{R} \quad (33)$$

In (33) k_m is the motor-constant of the VCM and R is the resistance of the coil in the VCM and U is the supplied voltage. The damping constant d due to back-emf is

$$d = \frac{k_m^2}{R} \quad (34)$$

The stiffness k is:

$$k = \frac{n \cdot 12 \cdot EI}{l^3} \quad (35)$$

In (35) E is Young's modulus of the spring material ($2.1 \cdot 10^{11}$ N/m²), I is the area moment of inertia, which is depending on the parameters of the cross-section of the leaf-springs, l is the length of the leaf-springs and $n = 2$ is the number of leaf-springs. From figure 2b the equation of motion can be obtained:

$$m \cdot \ddot{x} = -k \cdot x - d \cdot \dot{x} + \frac{U \cdot k_m}{R} \quad (36)$$

which leads to the transfer between applied voltage U and displacement of the mass x , $P(s)$ to read:

$$\frac{x(s)}{U(s)} = P(s) = \frac{\frac{k_m}{R \cdot m}}{s^2 + \frac{k_m^2}{R \cdot m} s + \frac{k}{m}} \quad (37)$$

The transfer function (37) perfectly matches the general transfer function of electro-mechanical systems as described by (2).

3.3.2 Controller type and required cross-over frequency

Figure 2 shows that in case of positioning the mass m , still a force is needed to compensate the spring even if the position error e (figure 6) is zero. As a consequence integral action should be needed.

Substitution of the controller transfer (??) and the process transfer (37) in the relation (32) results in the expression for the sensitivity function:

$$S(s) = \frac{s\tau_i(s\tau_p + 1)(s^2 + \frac{d}{m}s + \omega_1^2)}{s\tau_i(s\tau_p + 1)(s^2 + \frac{d}{m}s + \omega_1^2) + \frac{k_p \cdot k_m}{R \cdot m}(s\tau_z + 1)} \quad (38)$$

This expression for $S(s)$ (38) can be simplified giving the following assumptions. The cross-over frequency $\omega_c \gg \omega_1$ and $\omega_1 > \omega_{d2}$. $\omega_{d2} = 10 \cdot 2\pi$ rad/sec. is the worst-case disturbance frequency. In that case the disturbances are low frequent signals and consequently for analyses the low frequent approximation of $S(s)$ is adequate. The low frequent approximation of a transfer is found by taking only into account the lowest powers of s in both the denominator and nominator. This results in the $S_{LF}(s)$:

$$S_{LF}(s) = \frac{s \cdot \tau_i \cdot \omega_1^2}{\frac{k_p \cdot k_m}{R \cdot m}} \quad (39)$$

Figure 8 shows that (39) is at low frequencies an accurate approximation of (38). Figure 8 also shows that for a disturbance suppression of 10 Hz. the resonance frequency ω_1 could be best designed in the region 5Hz. to 18 Hz. However, we rely for the design on the low frequent asymptote of the sensitivity function. Substitution of the control-parameters as defined in (??) into (39) leads to:

$$S_{LF}(s) = \frac{2 \cdot \frac{1}{\alpha} \cdot \omega_1^2}{\omega_c^3} \cdot s \quad (40)$$

The specification prescribes that the amplitude of the disturbance due to vibration should be reduced in closed loop by a factor of 7. Therefore, this specification reads as:

$$S_{LF}(j \cdot \omega_d) = \frac{1}{7} = \frac{2 \cdot \frac{1}{\alpha} \cdot \omega_1^2}{\omega_c^3} \cdot j \cdot \omega_d \quad (41)$$

Consequently the cross-over frequency is determined by:

$$\omega_c = \sqrt[3]{7 \cdot \omega_1^2 \cdot \frac{2}{\alpha} \cdot \omega_d} \quad (42)$$

Equation 42 shows that the cross-over frequency is depending on the first resonance frequency, a choice for α and the frequency of the disturbance ω_d .

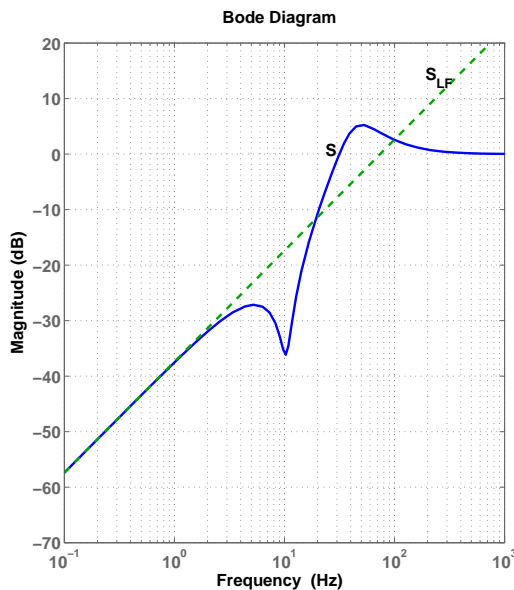


Figure 8: Bode plot of Sensitivity $|S|$

4 Dimensioning

4.1 Leaf-springs

Equation (42) parameterizes the problem. We can now dimension the leaf-springs and calculate the necessary controller parameters. After some iteration the following values are established. The head has a given weight of 0.44 kg (including the inductive sensor).

E	$2.1 \cdot 10^{11}$	N/m ²
length	0.030	m
width	0.015	m
d (thickn.)	0.0002	m
k	1866	N/m
ω_1	65	rad/sec.
ω_c	270	rad/sec.
α	0.2	

Table 1: Leaf-spring dimensions and control parameters

Some remarks on the dimensions shown in tabel 1. The length is the maximum allowable length given the restriction of the volume and the height of the (extended) head. The width of the leaf-springs is not a free choice. Because, one has to keep in mind that it determines the stiffness in not actuated directions.

So, it cannot be taken arbitrary small. It is decided to be 10 mm in an iterative proces where a trade-off between robust stability and stiffness in actuated direction has been made. The thickness cannot be chosen less. It is constrained by the laser cutting proces.

4.2 Voice coil actuator

Because a relatively good estimation of the stiffness in actuated direction is known and the displacement is known the actuator can be dimensioned. The displacement is taken, with some safety, to be ± 1 mm, so 2 mm in total. Due to the non-linear displacement behavior of VCM's the possible stroke of the actuator is advised to be at least twice the real displacement, so a stroke of 4 mm in order to keep the actual displacements in the area of linear behavior of the actuator.

The necessary maximum deformation force is:

$$F_d = 1.10^{-3} \cdot 1866 = 1.87N \quad (43)$$

The necessary maximum acceleration force:

$$F_a = m(\omega_{d1}^2 \cdot 0.3 \cdot 10^{-3} + \omega_{d2}^2 \cdot 0.4 \cdot 10^{-3}) = 0.56N \quad (44)$$

See tabel 2 for the chosen VCM from G⁺.

Type	VM 2618	
Length	18	mm
diameter	26	mm
k_m	3.2	N/A
R	9.6	Ohm
Stroke	4	mm
Moving mass	0.006	kg.
Stator mass	0.1	kg.
Cont. current	1.5	A
stator-rotor play	0.2	mm

Table 2: Voice Coil specs

4.3 Sensor

Due to the non-contact requirement, the sensor principle could either be optic, inductive or capacitive. Due to the relatively large gap and loose tolerances an inductieve sensor of Baumer type IWRM 08U9501 is chosen. Measurement stroke 2 mm. Resolution 5 μm ., repeatability 20 μm .

5 Three dimensional system modeling and analysis

Next a more tedious modeling task is necessary to find out the influences of the violation of exact constraint design, parasitic modes and their mode-shapes and restricted manufacturing tolerances on the (robust) stability of the closed loop.

In order to guarantee straight guidance in actuated direction the stiffness of the leaf-springs in all other directions must be relatively high in order to realize high frequent support modes. The latter are called parasitic modes. If the head is driven precisely in the line of the center of mass (c.o.m.), the parasitic modes are not excited and as a consequence they will not appear in the transfer from driving force to measurement output.

However, due to limitation in manufacturing one has to take into account a certain amount of misplacement of the actuator with respect to the c.o.m. The actuator is positioned in the center of the head itself, which does not coincide with the c.o.m of head en sensor combination. Moreover, in this case it is not possible to place the sensor at the principle-axis through the c.o.m. (c.o.m.-line) since the optics of the head are positioned in the c.o.m.-line. The sensor is placed 20 mm in negative x-direction and 8 mm in negative z-direction with respect to the origin which is in the center of the front-plane of the head (red-dot)(see figure 9 for the orientation of the axes). From a 3D point of view this implies non co-located control. Both constructive limitations result in the fact that some of the parasitic modes appear in the transfer from input-force to output.

We want to test robust stability of the closed loop system under influence of vibration modes. Therefore a model is needed which incorporates at least the modes expected to endanger stability.

SPACAR will be used to model the transfer functions. Figure 9 gives a rough sketch of the active head system including the support frames. It is a first guess to be checked, simple mechanical design issues can be applied for improvement. The frame parts 1 to 4 and the leafsprings are compliant. The head and sensor are considered rigid.

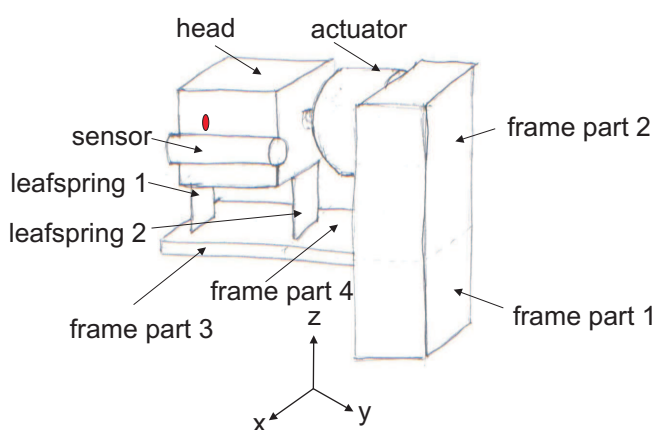


Figure 9: Sketch of the active head system

Figure 10 shows the SPACAR user interface input for the model resembling the conceptual design as in figure 9. The system is modeled using either flexible or rigid 3D beam elements and a 3D truss-element. The elements in group 1 represent the head, the sensor and the head-sensor connection. The beams represent the inertia properties of these construction elements²⁾. Connection beams are massless. The beams in this group or all rigid.

The elements in group 2 represent leafspring 1 end its connection to the head. The leafspring is modeled by two flexible beam-elements. The dimensions of the beams correspond with table 1³⁾.

The elements in group 3 represent leafspring 2 end its connection to the head. The elements in group 4 each represent an element of the 4 frame parts. These elements are flexible beam-elements.

The truss in group 5 is used to representing the actuator. The damping of the truss reflects the back-emf damping properties of the coil. The mass of the truss represent the coil mass. An additional point mass is added to frame part 2 to represent the stator mass of the actuator.

The only fixation point of the system is the base-point at the end of frame part 1. All deformations of the flexible beams are released. Remark that the leafsprings are modeled each by two elements. As a consequence the total deformation degrees of freedom of the flexible parts becomes 36 this should be added by the 6 degrees of freedom of the rigid body representing the head/sensor, which results in a total of 42 degrees of freedom. Remark that the internal damping of the applied material is assumed to be ≈ 0.01).

6 Analyses

SPACAR can compute the frequencies of the modes and can show the mode-shapes. Table 3 column 1 shows the frequencies of the modes and figure 11 shows the first four mode-shapes. The system is in it's initial unforced position.

The first mode represents the intended motion. The application of (31) results in $\omega_r = 6.3 \times \omega_c$. Therefore, the second and third mode are low frequent compared to the required cross-over frequency (43 Hz., table 1), as a consequence these modes might endanger closed loop stability. The second mode represents bending of frame part 3 and 4 and bending of the leafsprings in a direction perpendicular to the actuation and sensing direction. This mode is hardly excited by the actuator and has little or no contribution in the sensor-signal. It is therefore expected that the dynamics of this mode will appear in the transfer as a (nearby) pole-zero cancelation. The third mode consists of bending of frame parts 3 and 4 in sensor direction and bending of the leaf-springs in lateral direction. This mode is excited by the actuator and it is expected to have contribution in the sensor-signal.

To investigate the possible influence on robust stability of mode 2 and 3 the open-loop transfer from actuator force to sensor output is determined from the linearized model. Figure 12a shows the bode-magnitude plot of the transfer

²⁾The user-interface software automatically calculates the mass and inertia properties

³⁾The user-interface software automatically calculates the stiffness properties

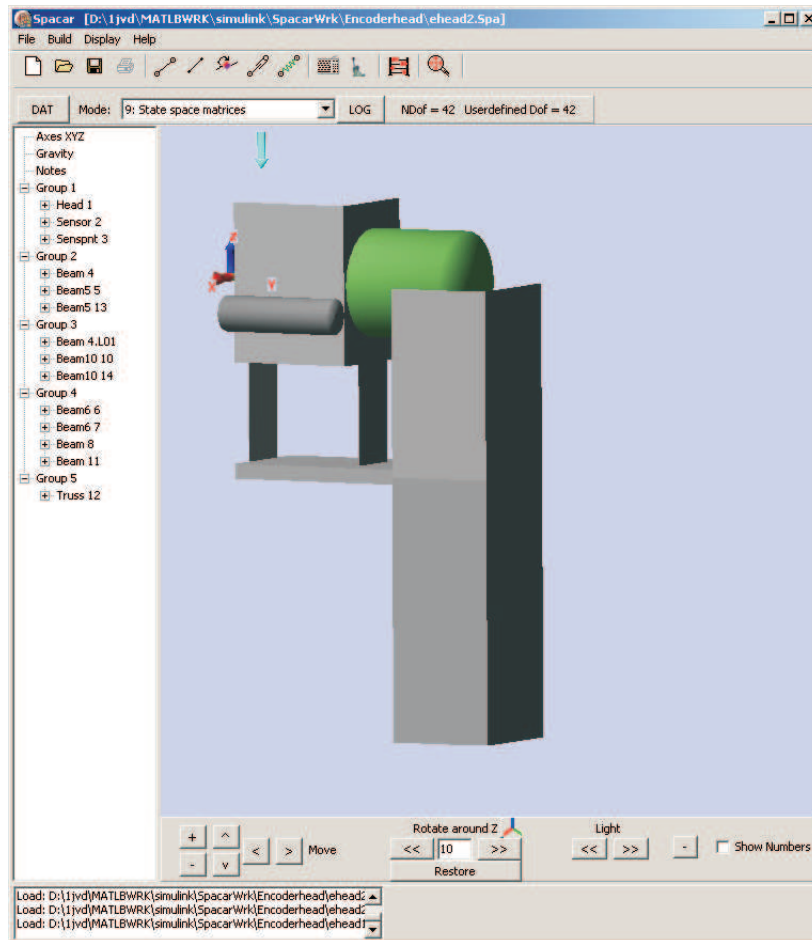


Figure 10: Spacar user-interface and model

$P(s)$ obtained via SPACAR and the inverse bode magnitude-plot of the PID⁺-controller $K(s)$ installing a cross-over frequency of 50 Hz. From figure 12a it is concluded that as expected mode 2 does not have influence and the influence of mode 3 is much less than initially expected. There is no violation of the robustness check (26).

However, next we are going to analyze the following situation. First, the system is loaded with an actuator force of 4 N. Which results in a displacement of the head in negative y-direction of 2.4 mm. Figure 12b shows the influence on the bode magnitude-plot ⁴⁾ of the transfer between actuator and sensor. Remark, the drop in frequency of the fourth mode (see column 2 in table 3). But there is no violation of robust stability.

Second, we are going to simulate the manufacturing tolerances. The construction as outlined violates exact constraint design⁵⁾. The rotational DOF of

⁴⁾The analyses take only a few seconds

⁵⁾Each leafspring suppresses 3 mobilities. As a consequence two leafsprings suppress 6 mobilities.

Mode	freq. Hz. unloaded	loaded sit- uation	imperfect aligned leafsprings	cut leaf- spring
1	10.4	10.4	11.6	10.1
2	118	114	87	95
3	208	195	135	218
4	675	385	216	324
5	1066			
6	1172			
7	1207			
8	1211			
9	1293			
10	1293			

Table 3: Mode frequencies

the head around the z-axis is closed twice, once by each leafspring. The head will move as expected as long as both leaf springs are perfectly parallel. A small imperfection, e.g. during manufacturing, will result in a different motion as the horizontal motion of the head may no longer involve pure bending of both leafsprings. This behavior can be simulated by imposing a rotation of 3 degrees around the z-axis at the base of leaf spring 1. It will imply different mode-shapes. The consequence is that mode 2 will be excited by the actuator and has a contribution in the sensor signal. Figure 12c shows the influence on the bode magnitude-plot of the transfer between actuator and sensor. Remark, the drop in frequency of the modes 2,3 and 4(see column 3 in table 3). The first mode is increased in frequency due to the stiffening of the leafsprings in y-direction during motion. Robust stability is violated.

To avoid the overconstrained design one of the leafsprings should be cut as already shown in figure 7c. With this proper design and no changes in loading and imperfect mounting the results on the robust stability are shown in figure 12d. The fourth column in table 3 shows the corresponding mode frequencies. The mode-shapes are of the same form as in the case without the imperfect mounting of the leaf spring 1.

7 Conclusions

A relationship between the frequency of higher order dynamics and the required control bandwidth, which is expressed by the required cross-over frequency, based on the small-gain theorem is presented. The relationship is important in mechatronic system design. The relationship needs 3D dynamic system modeling. It is applied to the design of a relatively simple problem. However, the example clearly shows that the amount of complexity is rapidly increased when considering the problem in 3 dimensional space. It is shown that limited manufacturing tolerances can be of great influence in a simple control problem. Often it leads to robust stability problems. However, proper exact constrained design

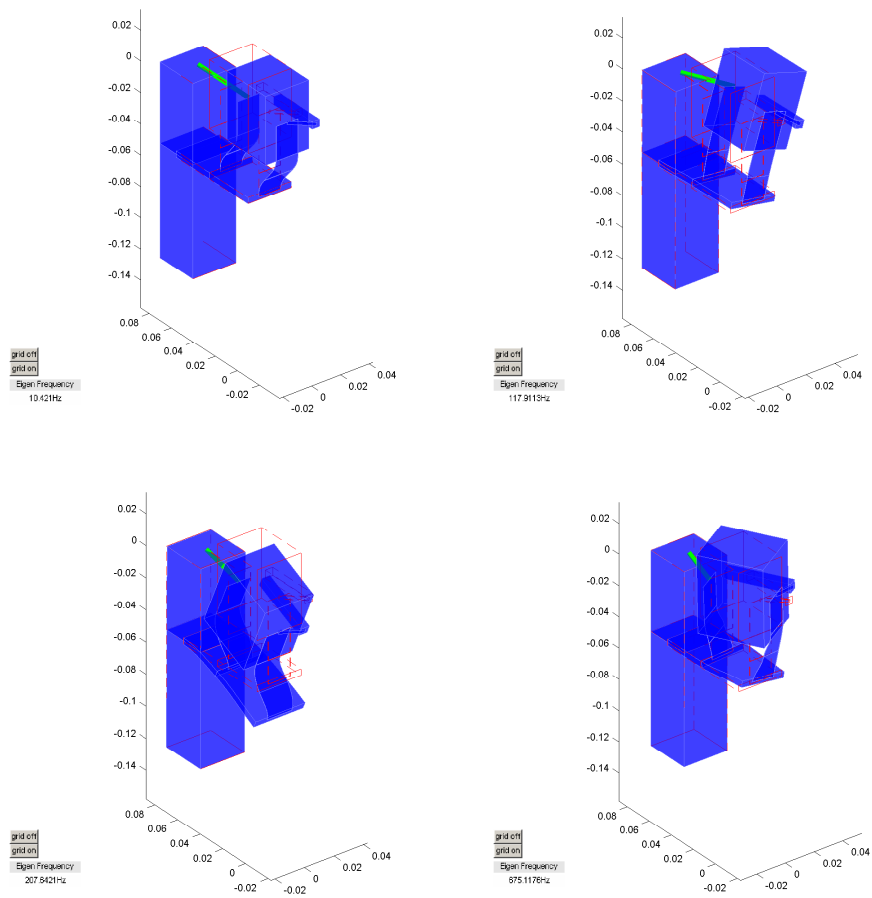


Figure 11: Mode-shapes of first four modes of the active head system

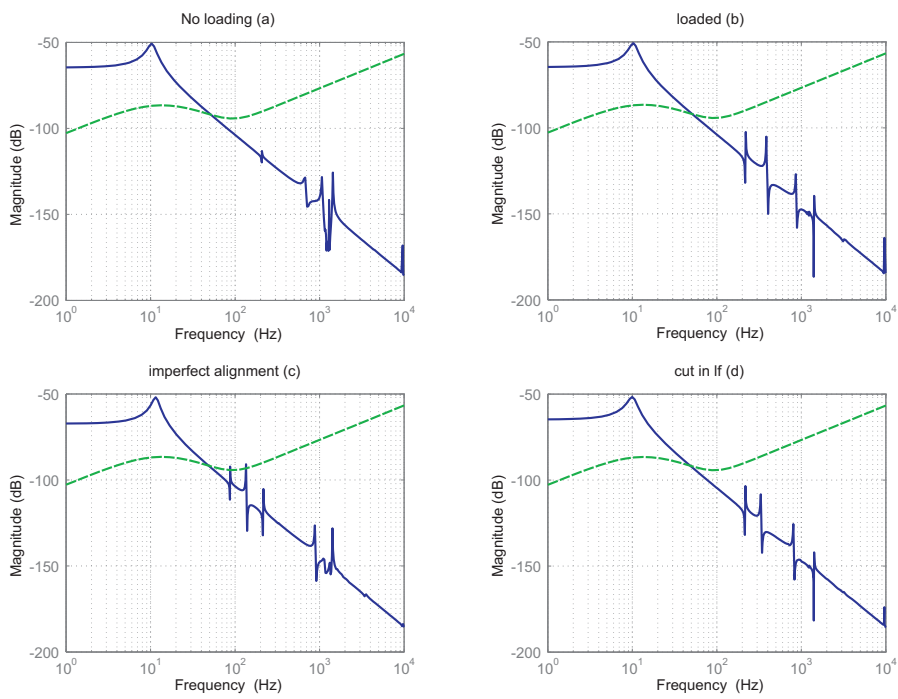


Figure 12: Small-gain robust stability check, unloaded situation(a), loaded situation(b),imperfect aligned leafsprings(c), one of the leafsprings is cut (d), shown is the bode magnitude plot of the inverse controller $C^{-1}(s)$ (dashed) and the process transfer $P(s)$ (solid)

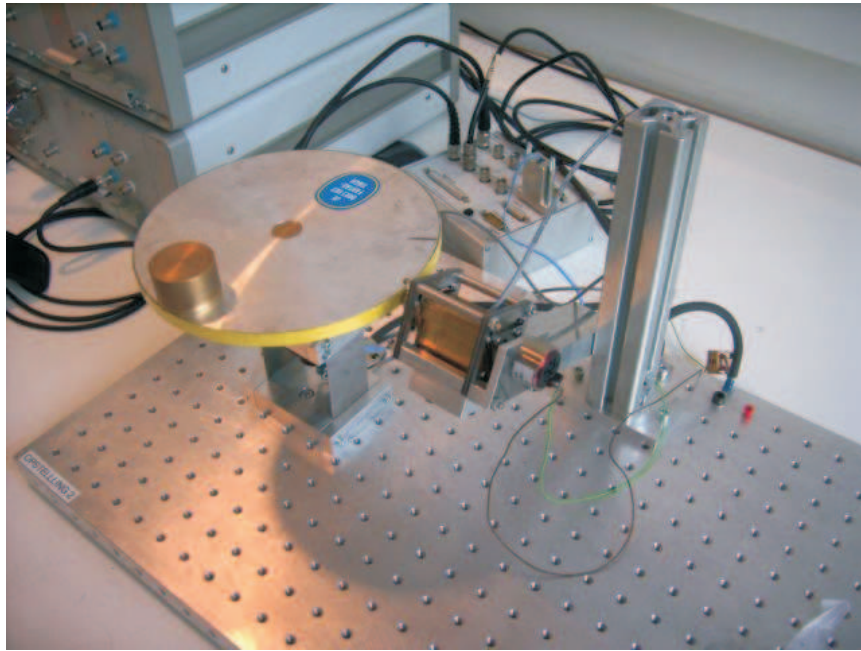


Figure 13: Photograph of realized setup

can cure the problem. This rather simple example system of a one degree of freedom (1-DOF) support mechanism with elastic leaf springs demonstrates the applicability of the SPACAR software for design considerations and for analyses of the non-linear behavior of the system. The formulation is based on a non-linear finite element description for flexible multibody systems. Flexible joints like flexure hinges and leaf springs can be modeled adequately using only a few number of flexible beam elements as these elements account for geometric non-linear effects such as geometric stiffening and interaction between deformation modes. In this way, a low dimensional system description can be obtained which is suitable for mechatronic design, i.e. the mechanical design as well as control system synthesis. It allows a designer to perform iterations quickly to optimize parameters.

References

- [1] The SPACAR software package, 2009. <http://www.spacar.nl/>.
- [2] D.L. Blanding. *Exact constraint: Machine design using kinematic processing*. Asme Press, New York, 1999 edition, 1999. ISBN 0-791-80085-7.
- [3] J. Dijk van. *Systems and control engineering*. University of Twente, jan. 2009 edition, 2009. code 113116 in dutch.
- [4] G.F. Franklin, J.D. Powell, and A. Emami-Naeini. *Feedback Control of Dynamic Systems*. Addison Wesley, 3rd edition, 1994. ISBN 0-201-53487-8.

- [5] Heidenhain. Angular encoders without integral bearing, <http://www.heidenhain.com>.
- [6] J.B. Jonker, R.G.K.M. Aarts, and J. van Dijk. "A linearized input-output representation of flexible multibody systems for control synthesis". *Multibody System Dynamics*, **21**:pp. 99–122, 2009.
- [7] S. Skogestad and I. Postlethwait. *Multivariable feedback control*. John Wiley, 1996 edition, 1996. ISBN 0-471-94277-4.